# Supplementary Information for

## Molecular subtypes of ALS are associated with differences in patient prognosis

Jarrett Eshima, Samantha A. O'Connor, Ethan Marschall, NYGC ALS Consortium, Robert Bowser, Christopher L. Plaisier, Barbara S. Smith

Correspondence to: BarbaraSmith@asu.edu

**This PDF file includes:**

Supplementary Text
Figs. S1 to S12

**Other Supplementary Materials for this manuscript include the following:**

Tables S1 to S14

## Supplementary Text

NYGC ALS Consortium Members and sites.

| # | Site | PI |
|---|---|---|
| 1 | Center for Genomics of Neurodegenerative Disease (CGND), New York Genome Center, New York, NY | Hemali Phatnani, PhD |
| 2 | Department of Neurology, Lewis Katz School of Medicine, Temple University, Philadelphia, PA | Justin Kwan, MD |
| 3 | Cedars-Sinai Department of Biomedical Sciences, Board of Governors Regenerative Medicine Institute and Brain Program, Cedars-Sinai Medical Center, and Department of Medicine, University of California, Los Angeles, CA | Dhruv Sareen, PhD |
| 4 | Department of Biochemistry and Molecular Biology, Penn State Institute for Personalized Medicine, The Pennsylvania State University, Hershey, PA | James R. Broach, PhD |
| 5 | Department of Neurology, The Pennsylvania State University, Hershey, PA | Zachary Simmons, MD |
| 6 | Department of Neurology, Henry Ford Health System, Detroit, MI | Ximena Arcila-Londono, MD |
| 7 | Department of Pathology and Laboratory Medicine, Perelman School of Medicine, University of Pennsylvania, Philadelphia, PA | Edward B. Lee, MD, PhD |
| 8 | Department of Pathology and Laboratory Medicine, Perelman School of Medicine, University of Pennsylvania, Philadelphia, PA | Vivianna M. Van Deerlin, MD, PhD |
| 9 | Department of Neurology, Center for Motor Neuron Biology and Disease, Institute for Genomic Medicine, Columbia University, New York, NY | Neil A. Shneider, MD, PhD |
| 10 | Department of Biological Engineering, Massachusetts Institute of Technology, Cambridge, MA | Ernest Fraenkel, PhD |
| 11 | Department of Neurology, Johns Hopkins School of Medicine, Baltimore, MD | Lyle W. Ostrow, MD, PhD |
| 12 | Department of Neurogenetics, Academic Medical Centre, Amsterdam and Leiden University Medical Center, Leiden, The Netherlands | Frank Baas, MD, PhD |
| 13 | Department of Medicine, Lung Biology Center, University of California, San Francisco, CA | Noah Zaitlen, PhD |
| 14 | ALS Multidisciplinary Clinic, Neuromuscular Division, Department of Neurology, Harvard Medical School, and Neurological Clinical Research Institute, Massachusetts General Hospital, Boston, MA | James D. Berry, MD, MPH |
| 15 | Centre for Neuroscience and Trauma, Blizard Institute, Barts and The London School of Medicine and Dentistry, Queen Mary University of London, London, and Department of Neurology, Basildon University Hospital, Basildon, United Kingdom | Andrea Malaspina, MD, PhD |
| 16 | Institute of Neurology, National Hospital for Neurology and Neurosurgery, University College London, London, United Kingdom | Pietro Fratta, MD, PhD |
| 17 | The Jackson Laboratory, Bar Harbor, ME | Gregory A. Cox, PhD |
| 18 | Department of Psychiatry & Human Behavior, Department of Biological Chemistry, School of Medicine, and Department of Neurobiology and Behavior, School of Biological Sciences, University California, Irvine, CA | Leslie M. Thompson, PhD |
| 19 | Taube/Koret Center for Neurodegenerative Disease Research, Roddenberry Center for Stem Cell Biology and Medicine, Gladstone Institute | Steve Finkbeiner, MD, PhD |
| 20 | Department of Neurology & Sensory Organs, University of Thessaly, Thessaly, Greece | Efthimios Dardiotis, MD, PhD |
| 21 | Department of Neurology, Washington University in St. Louis, St. Louis, MO | Timothy M. Miller, MD, PhD |
| 22 | Centre for Clinical Brain Sciences, Anne Rowling Regenerative Neurology Clinic, Euan MacDonald Centre for Motor Neurone Disease Research, University of Edinburgh, Edinburgh, United Kingdom | Siddharthan Chandran, PhD |
| 23 | Centre for Clinical Brain Sciences, Anne Rowling Regenerative Neurology Clinic, Euan MacDonald Centre for Motor Neurone Disease Research, University of Edinburgh, Edinburgh, United Kingdom | Suvankar Pal, MD |
| 24 | Department of Molecular Genetics, Weizmann Institute of Science, Rehovot, Israel | Eran Hornstein, MD, PhD |
| 25 | Department of Neurology, Icahn School of Medicine at Mount Sinai, New York, NY | Daniel J. MacGowan, MD |
| 26 | Center for Neurodegenerative Disorders, Department of Neurology, the Lewis Katz School of Medicine, Temple University, Philadelphia, PA | Terry Heiman-Patterson, MD |
| 27 | Cold Spring Harbor Laboratory, Cold Spring Harbor, NY | Molly G. Hammell, PhD |

| | | |
|---|---|---|
| 28 | Computer Science and Systems Biology Program, Ann Romney Center for Neurological Diseases, Department of Neurology and Division of Genetics in Department of Medicine, Brigham and Women's Hospital, Boston, MA, Harvard Medical School, Boston, MA, and Program in Medical and Population Genetics, Broad Institute, Cambridge, MA | Nikolaos. A. Patsopoulos, MD, PhD |
| 29 | Ann Romney Center for Neurologic Diseases, Brigham and Women's Hospital, Harvard Medical School, Boston, MA | Oleg Butovsky, PhD |
| 30 | Department of Anesthesiology, Stony Brook University, Stony Brook, NY | Joshua Dubnau, PhD |
| 31 | Section of Infections of the Nervous System, National Institute of Neurological Disorders and Stroke, NIH, Bethesda, MD | Avindra Nath, MD |
| 32 | Department of Neurology, Barrow Neurological Institute, St. Joseph's Hospital and Medical Center, Department of Neurobiology, Barrow Neurological Institute, St. Joseph's Hospital and Medical Center, Phoenix, AZ | Robert Bowser, PhD |
| 33 | Department of Neurology, Division of Neuromuscular Medicine, Columbia University, New York, NY | Matthew Harms, MD |
| 34 | Department of Neuropathology, Academic Medical Center, University of Amsterdam, Amsterdam, The Netherlands | Eleonora Aronica, MD, PhD |
| 35 | Department of Biology and Veterinary and Biomedical Sciences, The Pennsylvania State University, University Park, PA | Mary Poss, DVM, PhD |
| 36 | New York Stem Cell Foundation, Department of Bioengineering, School of Engineering and Applied Sciences, University of Pennsylvania, Philadelphia, PA | Jennifer Phillips-Cremins, PhD |
| 37 | Department of Pathology, Fishberg Department of Neuroscience, Friedman Brain Institute, Ronald M. Loeb Center for Alzheimer's Disease, Icahn School of Medicine at Mount Sinai, New York, NY | John Crary, MD, PhD |
| 38 | Department of Neurology, Harvard Medical School, Neurological Clinical Research Institute, Massachusetts General Hospital, Boston, MA | Nazem Atassi, MD |
| 39 | Department of Neurology, Hospital for Special Surgery and Weill Cornell Medical Center, New York, NY | Dale J. Lange, MD |
| 40 | Medical Genetics, Atlantic Health System, Morristown Medical Center, Morristown, NJ, and Overlook Medical Center, Summit, NJ | Darius J. Adams, MD |
| 41 | Center of Clinical Research, Experimental Surgery and Translational Research, Biomedical Research Foundation of the Academy of Athens (BRFAA), 4 Soranou Efesiou Street, 11527, Athens, Greece; 1st Department of Neurology, Eginition Hospital, Medical School, National and Kapodistrian University of Athens, Athens, Greece | Leonidas Stefanis, MD, PhD |
| 42 | Neuromuscular/EMG service and ALS/Motor Neuron Disease Clinic, Hebrew University-Hadassah Medical Center, Jerusalem, Israel | Marc Gotkine, MBBS |
| 43 | Board of Governors Regenerative Medicine Institute, Los Angeles, CA; Department of Neurology, Cedars-Sinai Medical Center, Los Angeles, CA | Robert H. Baloh, MD, PhD |
| 44 | Neurological Clinical Research Institute, Massachusetts General Hospital, Boston, MA | Suma Babu, MBBS, MPH |
| 45 | Departments of Neuroscience, and Genetics and Genomic Sciences, Ronald M. Loeb Center for Alzheimer's disease, Icahn School of Medicine at Mount Sinai, New York, NY | Towfique Raj, PhD |
| 46 | Harvard Medical School, Department of Physical Medicine & Rehabilitation, Spaulding Rehabilitation Hospital, Boston, MA | Sabrina Paganoni, MD, PhD |
| 47 | Center for Cellular and Molecular Therapeutics, Children's Hospital of Philadelphia, Philadelphia, PA; Department of Genetics, Perelman School of Medicine, University of Pennsylvania, Philadelphia, PA | Ophir Shalem, PhD |
| 48 | Centre for Clinical Brain Sciences, University of Edinburgh, Edinburgh, UK; Euan MacDonald Centre for Motor Neurone Disease Research, University of Edinburgh, Edinburgh, UK | Colin Smith, MD |
| 49 | Department of Genetics and Genomic Sciences, Icahn Institute of Data Science and Genomic Technology, Icahn School of Medicine at Mount Sinai, New York, NY | Bin Zhang, PhD |
| 50 | University of Maryland Brain and Tissue Bank and NIH NeuroBioBank | |
| 51 | Department of Neuropathology, Georgetown Brain Bank, Georgetown Lombardi Comprehensive Cancer Center, Georgetown University Medical Center, Washington DC | Brent Harris, MD, PhD |
| 52 | Neuroradiology Section, Department of Radiology and Biomedical Imaging, University of California, San Francisco, San Francisco, CA | Iris Broce, PhD |

53 Neuromuscular Diseases Unit, Department of Neurology, Tel Aviv Sourasky Medical Center, Sackler Faculty of Medicine, Tel-Aviv University, Tel-Aviv, Israel — Vivian Drory, MD
54 Department of Neuroscience, University of California San Diego, La Jolla, CA — John Ravits, MD
55 Department of Neurology, University of Pennsylvania Perelman School of Medicine, Philadelphia, PA — Corey McMillan, PhD
56 Department of Neurology, Columbia University Medical Center, New York, NY — Vilas Menon, PhD

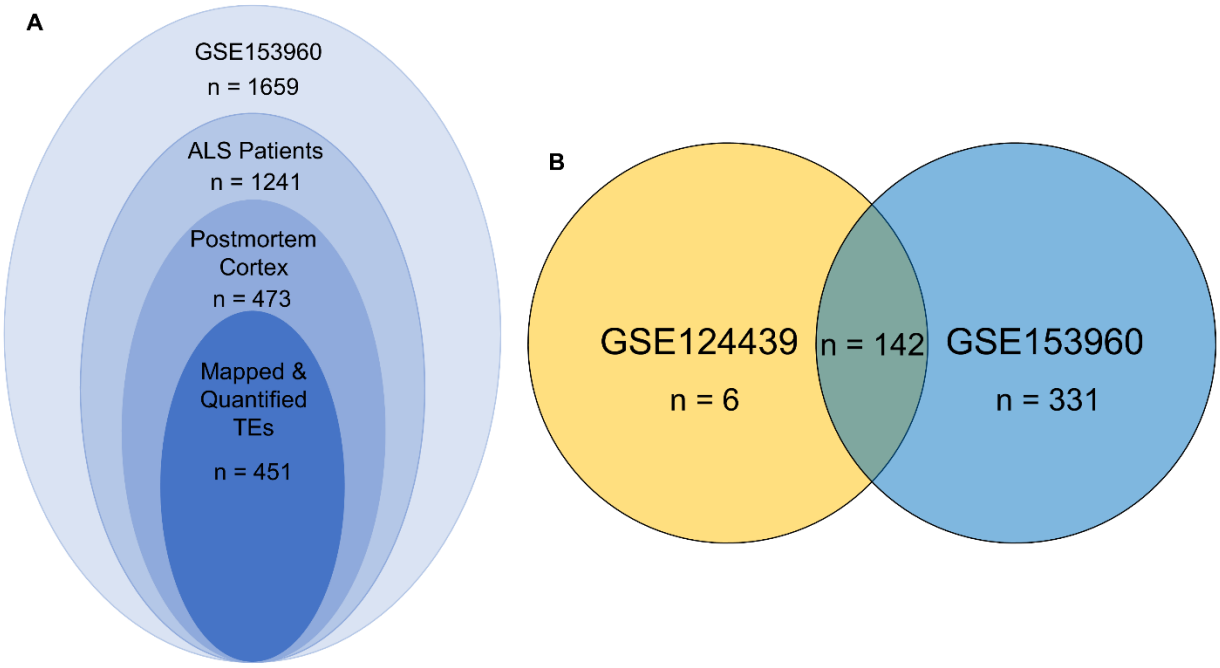


**Fig. S1. Overview of the ALS cohort**

(**A**) Selection of our ALS cohort from the GSE153960 repository. Transcriptomes associated with the frontal and motor cortex were the only tissue sites considered in this analysis. Control samples are not shown, but included 93 transcriptomes from healthy control donors and 42 from frontotemporal lobar degeneration patients. (**B**) Comparison of common ALS patient postmortem cortex samples between the foundational study from Tam et al. (GSE124439) and the repository utilized in this analysis.

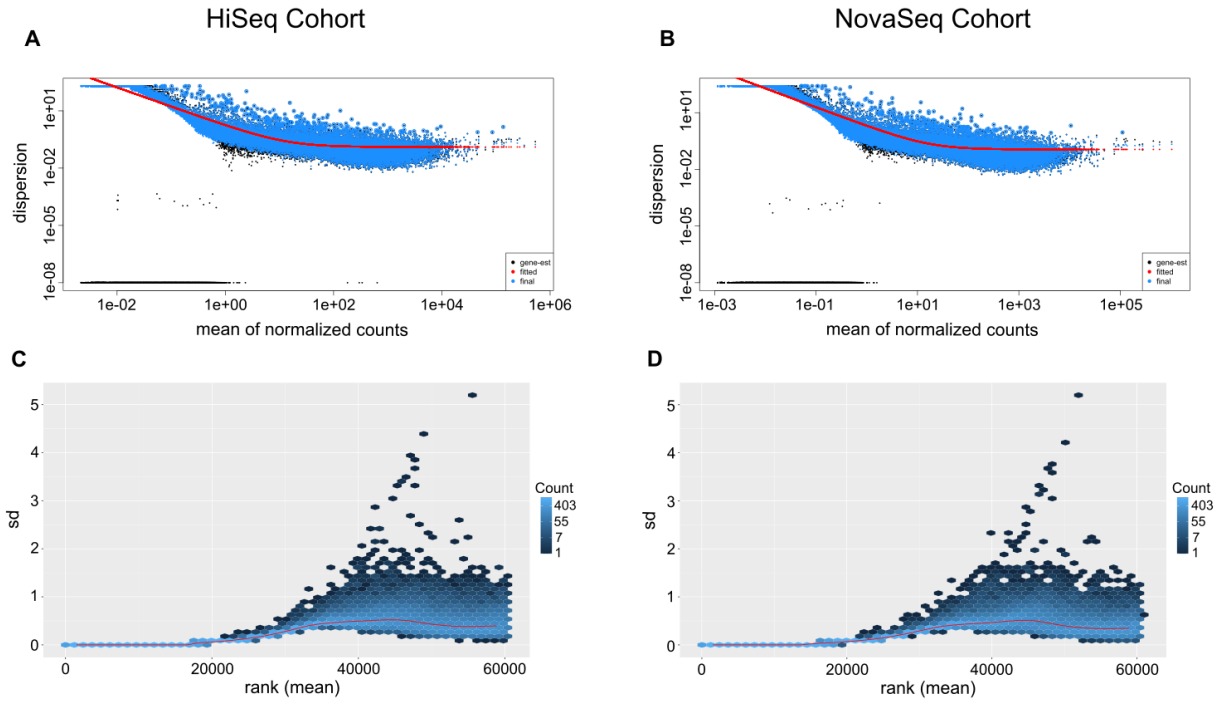


**Fig. S2. DESeq2 normalization metrics**

(**A**) Dispersion estimation for transcript counts in the HiSeq ALS cohort show gene-wise estimates shrunken towards the fitted estimates. (**B**) Dispersion estimation for transcript counts in the NovaSeq ALS cohort. (**C**) Variance stabilized, mean-standard deviation plot shows roughly the same standard deviation in transcript counts, regardless of gene rank, for the HiSeq ALS cohort. (**D**) Similar standard deviation magnitudes are observed in the variance stabilized, mean-standard deviation plot for the NovaSeq ALS cohort.

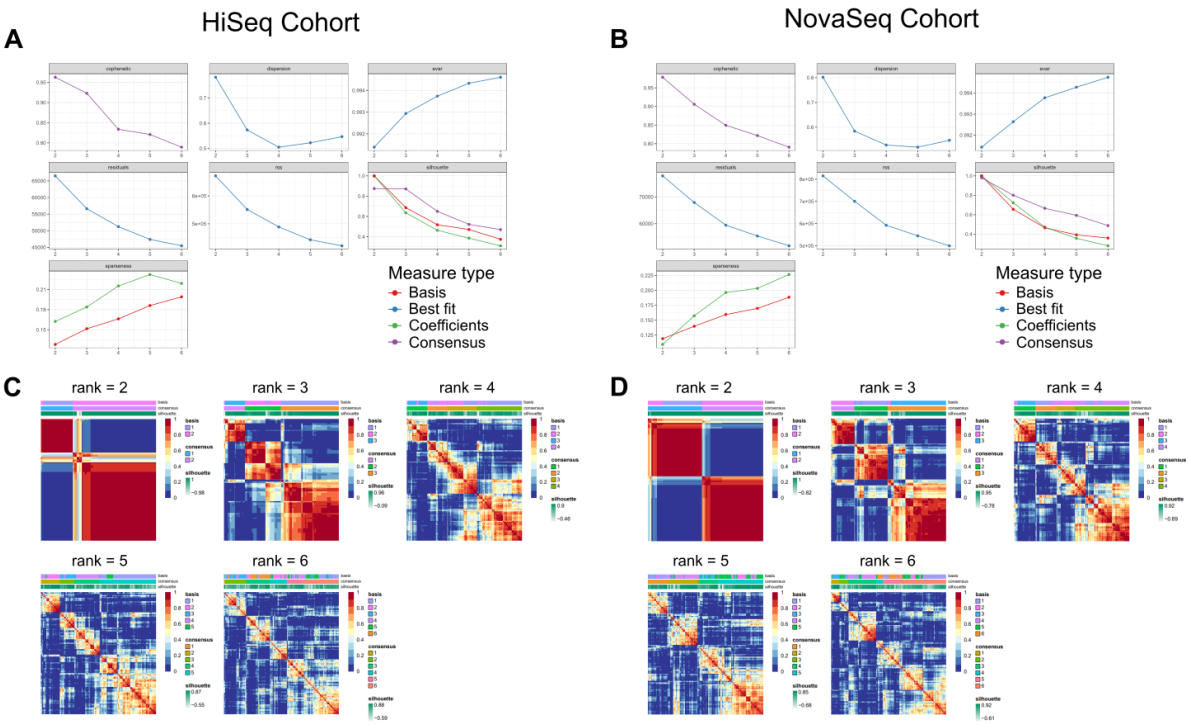


**Fig. S3. Estimation of factorization rank**

Preliminary unsupervised clustering analysis indicated a factorization rank of 3 was optimal for both the NovaSeq and HiSeq cohorts. (**A**) Non-smooth non-negative matrix factorization metrics for ranks 2-6 in the HiSeq cohort. (**B**) Clustering metrics are shown for the NovaSeq ALS cohort, spanning ranks 2-6. (**C**) Consensus clustering was performed for each rank considered in the HiSeq cohort. (**D**) Consensus clustering results are shown for ranks 2-6 in the NovaSeq cohort.

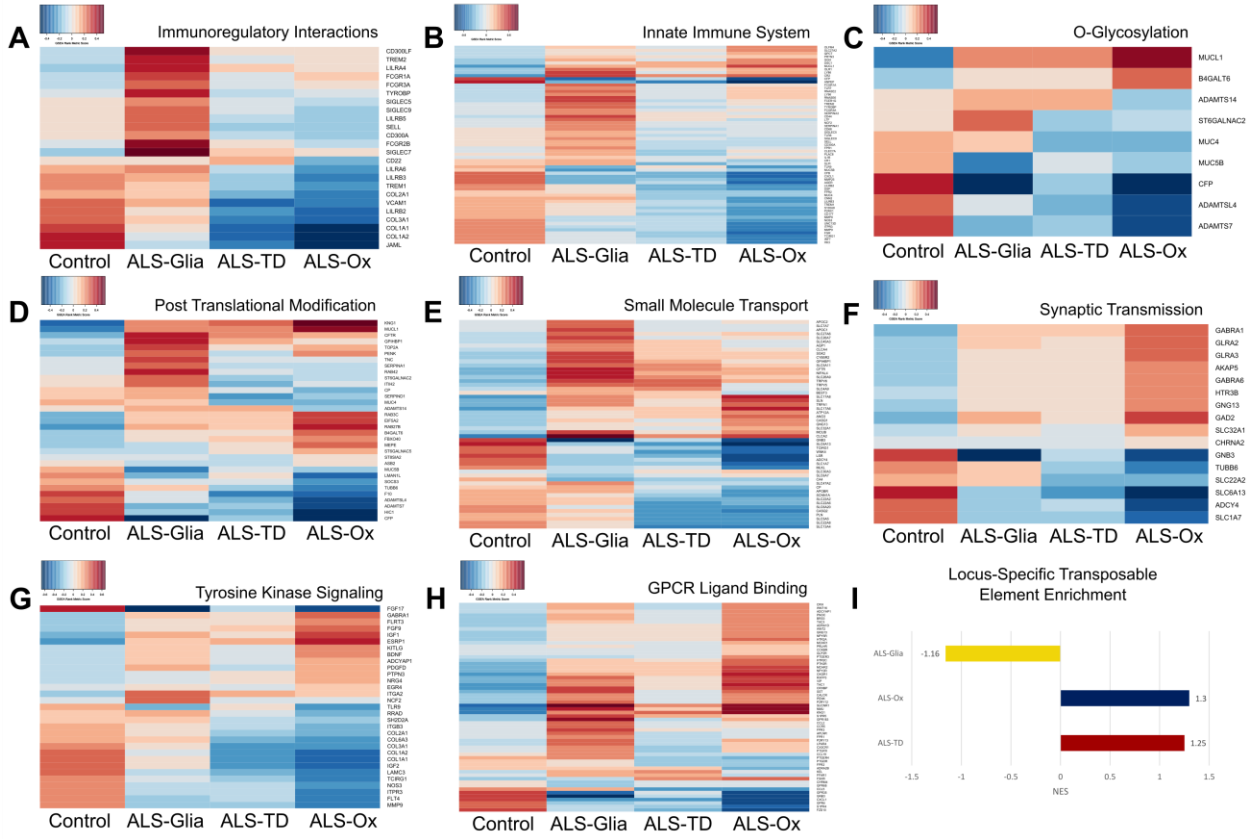


**Fig. S4. Enrichment heatmaps supporting subtype-dependent ALS phenotypes**

(**A**-**B**) The ALS-Glia subtype shows unique enrichment for pathways related to the immune system, as compared to healthy controls. (**C**-**D**) O-glycosylation and post translational modification machinery are altered in ALS patients. (**E**-**H**) Enrichment for synaptic signaling and neuronal receptor signaling pathways in the ALS-Ox subtype shows distinct expression, as compared to healthy controls. (**I**) A locus-specific transposable element feature set, derived from SQuIRE[13], was utilized to perform TE enrichment using GSEA. Normalized enrichment scores for each of the three subtypes are plotted, with healthy controls specified as the reference. Results indicate that elevated expression of TEs are characteristic of both the ALS-Ox and ALS-TD subtypes.

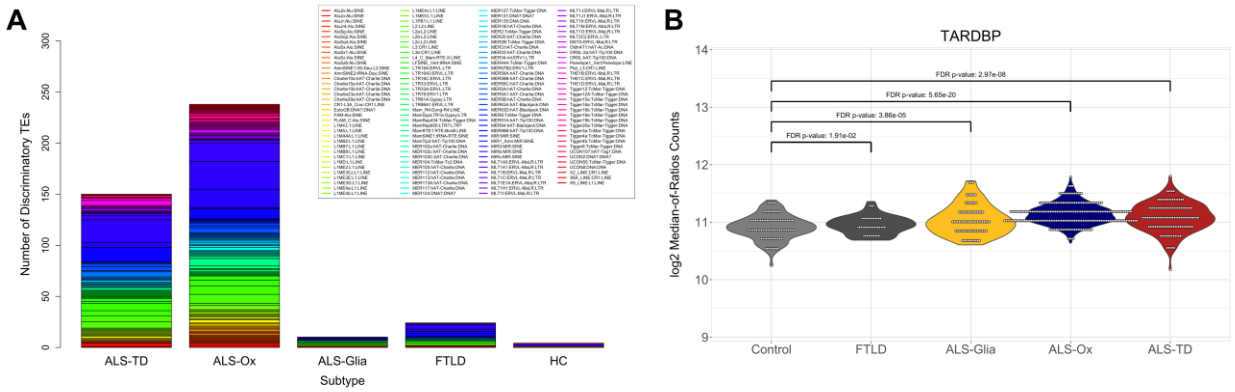


**Fig. S5. Consideration of locus-specific transposable elements in ALS spectrum neurodegeneration**

(**A**) Locus-specific transposable elements were assigned to the group which demonstrated the largest average expression on the median-of-ratios scale, and reveals characteristic expression in both the TD and Ox subtypes. (**B**) *TARDBP* expression, encoding TDP-43, is shown for healthy controls, patients with frontotemporal degeneration, and each ALS subtype on the DESeq2 median-of-ratios scale. Previous works have demonstrated direct interactions between TDP-43 and transposable elements (TEs) and implicated TE subfamilies as subtype specific features[7], however normalized expression is relatively consistent across ALS subtypes, suggesting *TARDBP* expression is not a defining characteristic of a single subtype.

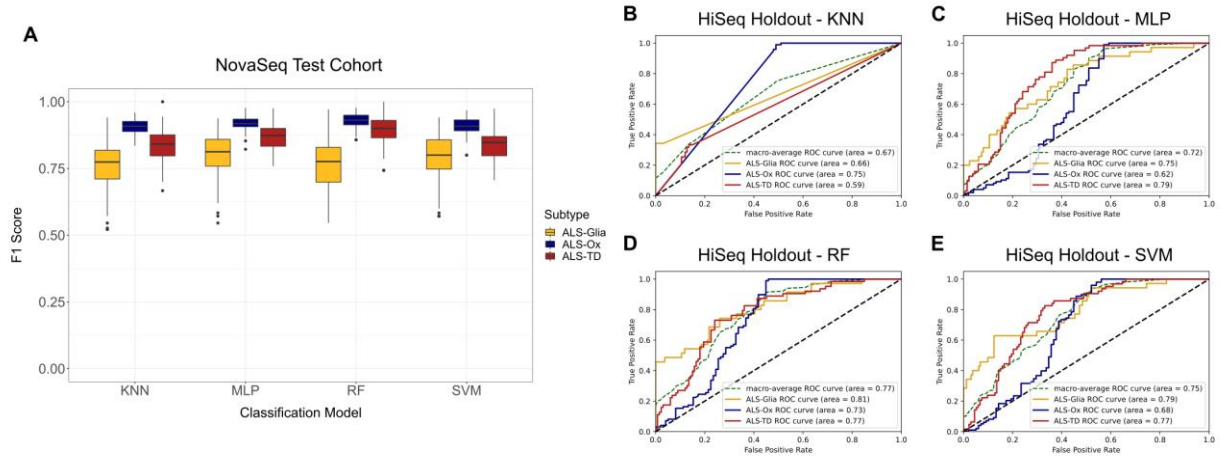


**Fig. S6. Performance of four supervised machine learning classifiers in the ALS cohort**

(A) F1 scores from 100-fold cross validation with the NovaSeq cohort are shown as boxplots. Four classification methods were considered (KNN, MLP, RF, and linear SVC) and predictive metrics are separated by subtype label. The MLP classifier demonstrated the highest average F1 score for the ALS-Glia subtype (0.80), while the RF classifier showed the best performance when predicting the ALS-Ox (0.93) and ALS-TD subtypes (0.90). (B) ROC plot showing false positive rate (1-specificity) versus the true positive rate (sensitivity) for the KNN classifier when applied to the holdout (HiSeq) cohort. Given the multi-class nature of this analysis, three classifiers were constructed accounting for each binary case, using a 'one-versus-rest' approach. (C) ROC plot showing predictive metrics for the MLP classifier. (D) Sensitivity and specificity metrics for the random forest classifier when applied to the holdout cohort. (E) ROC plot for the linear SVM classifier show similar performance to the RF and MLP models.

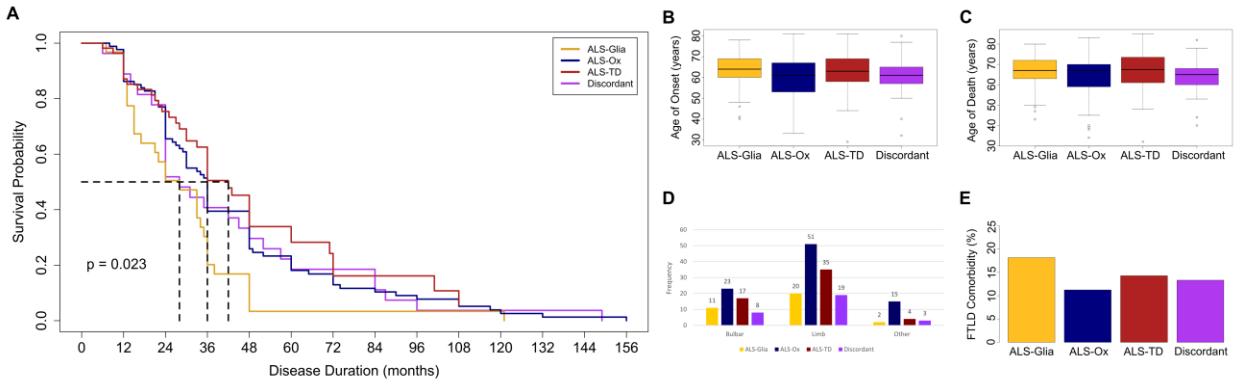


**Fig. S7. Inclusion of discordant patients when assessing clinical parameters**

(**A**) Kaplan-Meier survival analysis including the three ALS subtypes and 'discordant' patients. Pairwise comparisons showed significant differences in survival between the ALS-Glia and ALS-Ox subtypes ($p$ = 0.015) and ALS-Glia and ALS-TD subtypes ($p$ = 0.0043). (**B**) Age of ALS symptom onset are plotted as boxplots, separated by disease group. The ALS-Glia subtype shows a nonsignificant trend towards the latest symptom onset. (**C**) Age at death are shown for the three ALS subtypes and discordant patients. (**D**) Site of symptom onset are shown for all ALS patients included in this analysis, and a chi-square test of independence suggests site of symptom onset and subtype are not strongly associated. The 'other' category is comprised of axial (4), axial-limb (2), bulbar-limb (4), axial-bulbar (2), generalized (1), and unknown (11) sites of onset. (**E**) Frontotemporal lobar degeneration comorbidity is shown as a percentage, for all ALS patient groups considered in this analysis. A chi-square test of independence again suggests FTLD comorbidity and ALS subtype are not strongly associated.

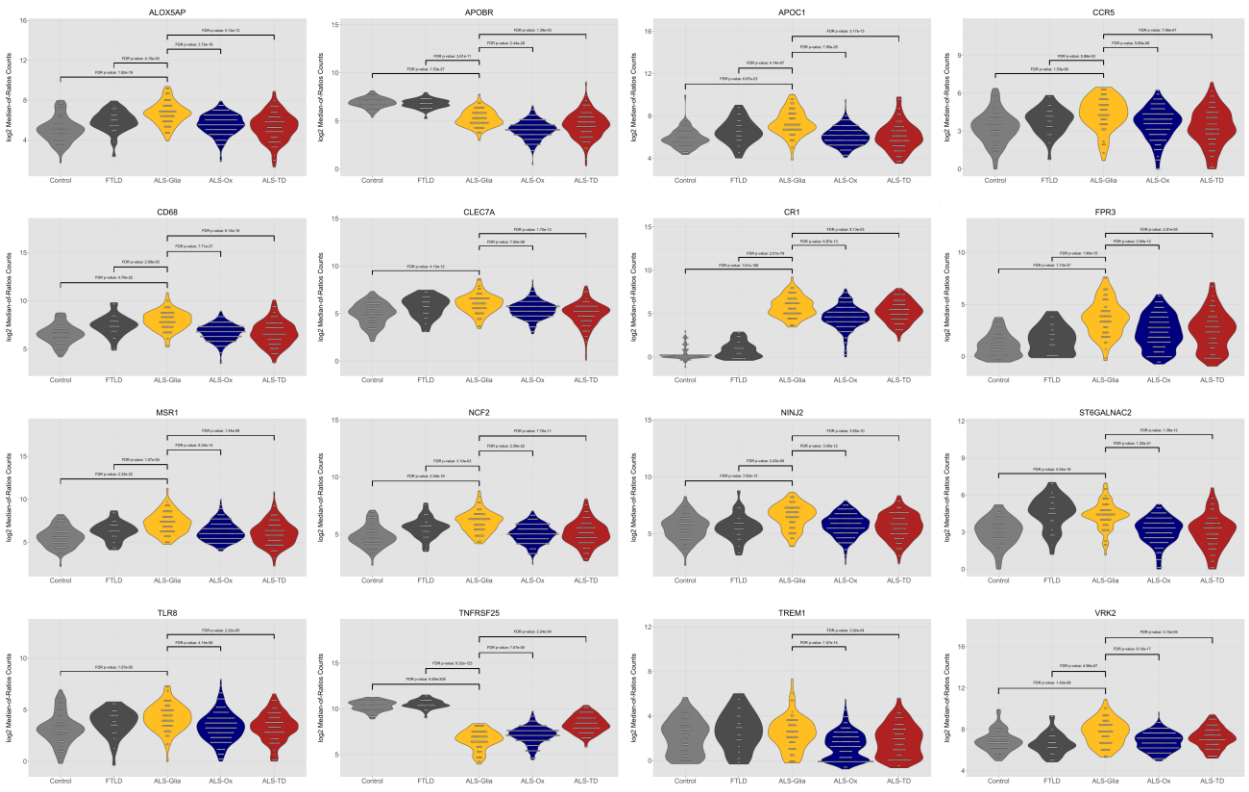


**Fig. S8. Supporting features for the ALS-Glia subtype**

Violin plots show ALS-Glia specific expression for 16 supporting genes: (*top left)* *ALOX5AP*, *APOBR*, *APOC1*, *CCR5*, *CD68*, *CLEC7A*, *CR1*, *FPR3*, *MSR1*, *NCF2*, *NINJ2*, *ST6GALNAC2*, *TLR8*, *TNFRSF25*, *TREM1*, and *VRK2*. Genes are generally associated with glial activation, neuroinflammation, and a pro-apoptotic phenotype.

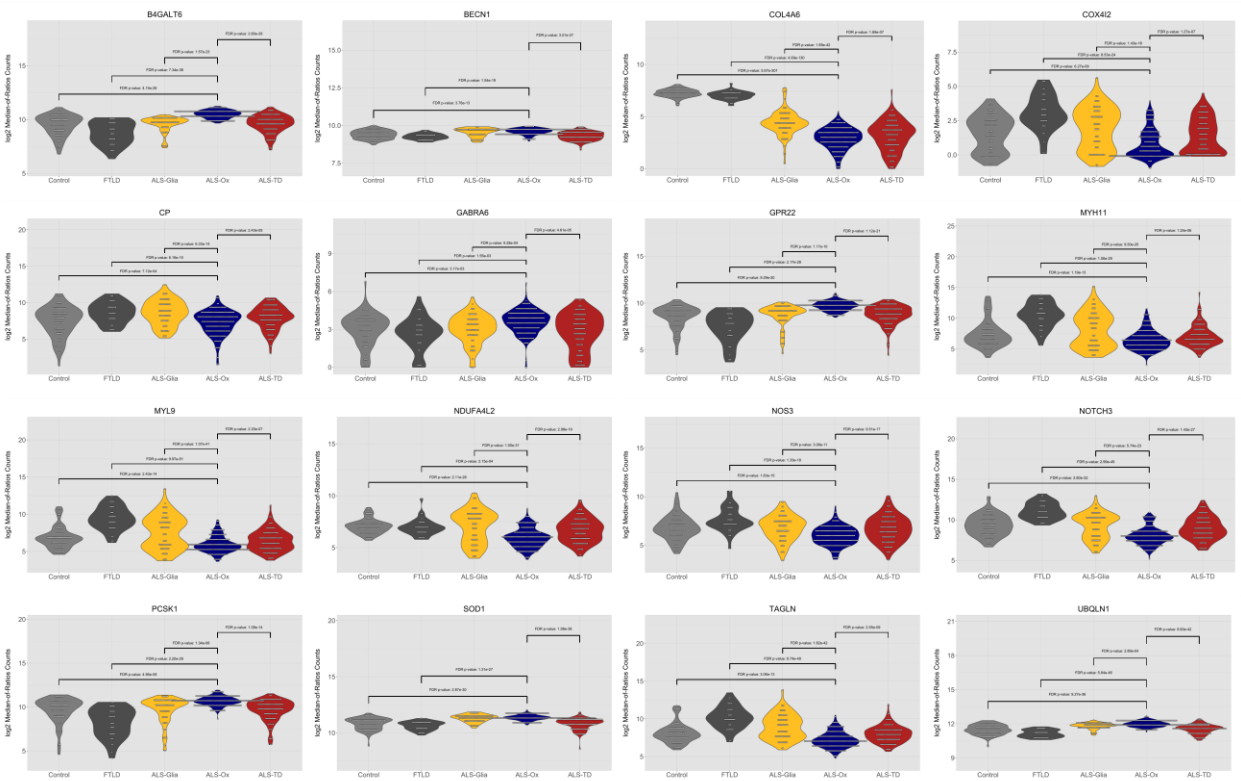


**Fig. S9. Supporting features for the ALS-Ox subtype**

ALS-Ox specific gene expression is shown as violin plots, and include: (*top left*) *B4GALT6*, *BECN1*, *COL4A6*, *COX4I2*, *CP*, *GABRA6*, *GPR22*, *MYH11*, *MYL9*, *NDUFA4L2*, *NOS3*, *NOTCH3*, *PCSK1*, *SOD1*, *TAGLN*, and *UBQLN1*. Supporting genes are generally associated with synaptic signaling, blood-brain barrier integrity, oxidative stress, and proteotoxic stress.

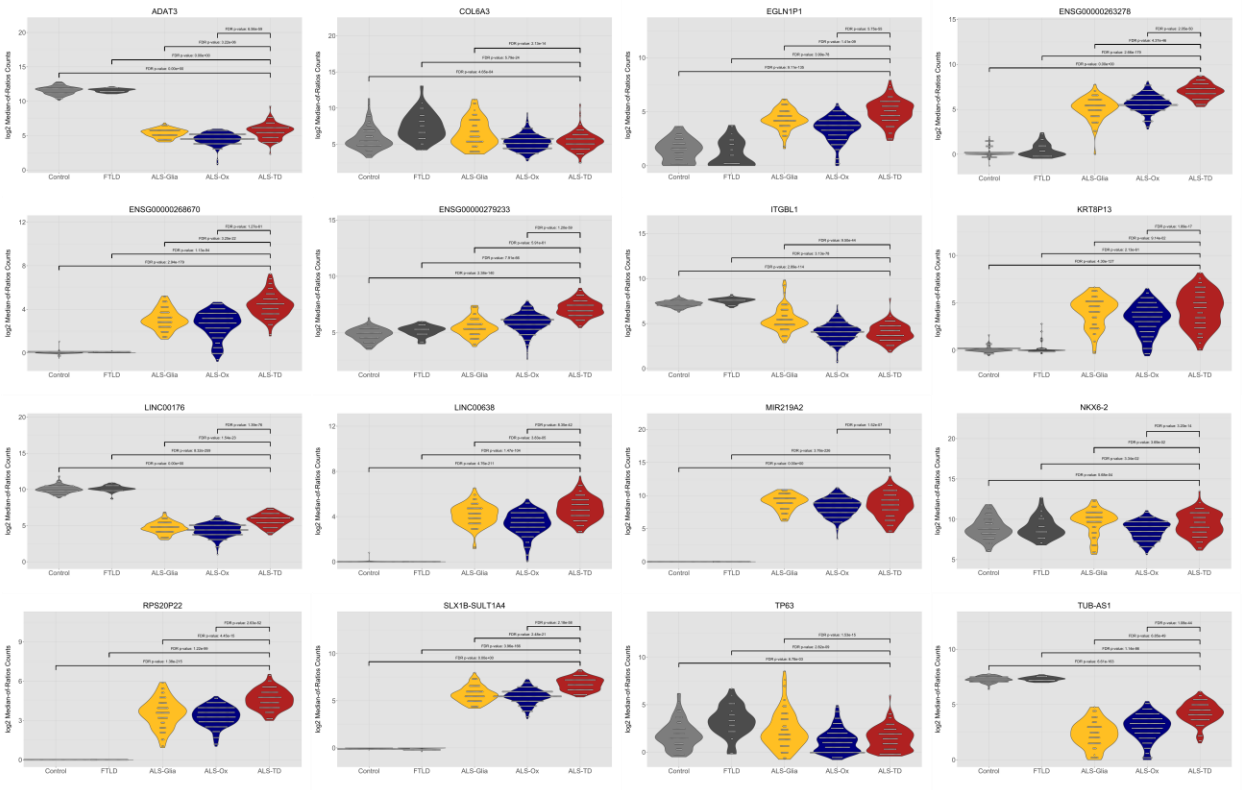


**Fig. S10. Supporting features for the ALS-TD subtype**

ALS-TD specific feature expression is shown as violin plots, and include: (*top left*) *ADAT3*, *COL6A3*, *EGLN1P1*, *ENSG00000263278*, *ENSG00000268670*, *ENSG00000279233*, *ITGBL1*, *KRT8P13*, *LINC00176*, *LINC00638*, *MIR219A2*, *NKX6-2*, *RPS20P22*, *SLX1B-SULT1A4*, *TP63*, and *TUB-AS1*. Supporting genes are generally associated with transcriptional regulation.

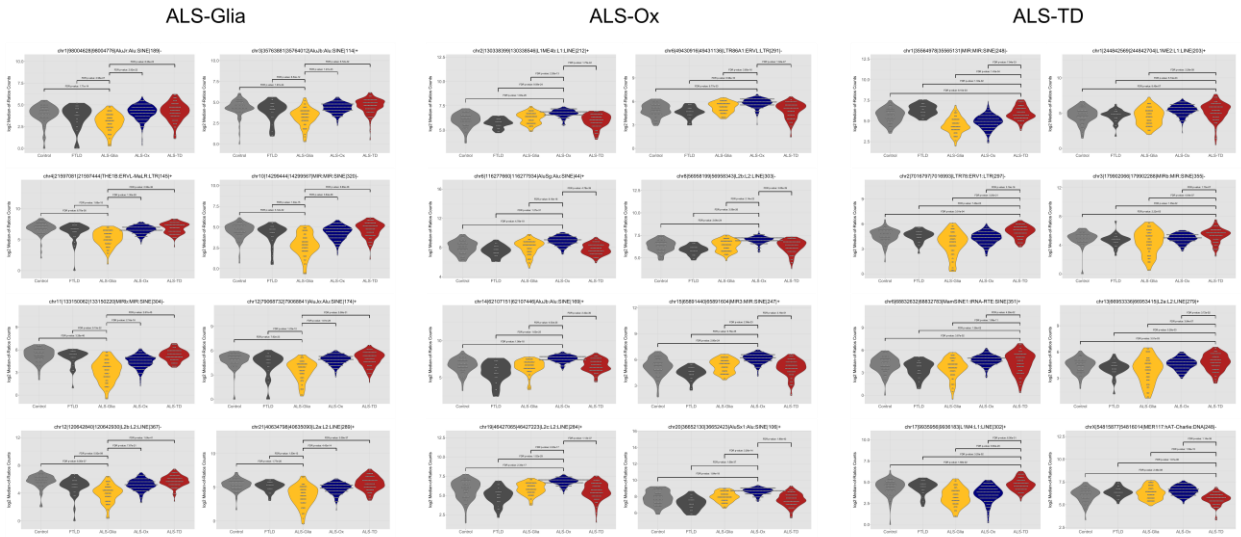


**Fig. S11. Subtype-specific transposable element expression**

Representative TE features for the ALS-Glia, ALS-Ox, and ALS-TD subtypes. ALS-Ox and ALS-TD subtypes were defined by upregulated expression of long interspersed nuclear elements (LINEs), short interspersed nuclear elements (SINEs), and long terminal repeats (LTRs). The ALS-Glia subtype was defined by downregulated expression of TEs, as compared to other ALS subtypes and controls.

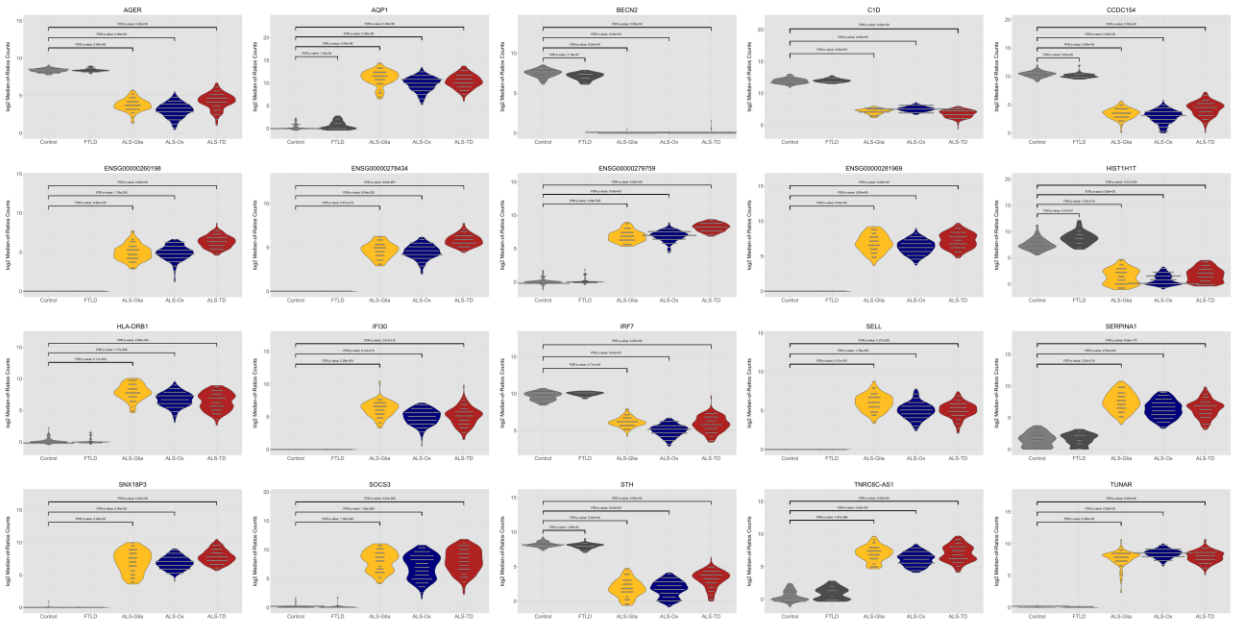


**Fig. S12. Characteristic gene expression distinguishes ALS patients from controls**

Genes strongly differentially expressed between ALS patients and controls. Violin plots indicate simple thresholding could be utilized to distinguish ALS patients from controls and some genes further show subtype-specific upregulation or downregulation. Of notable interest, elevated expression of *STH* in the brain is known to serve as a marker for Parkinson's and other neurodegenerative diseases, including FTLD, and is observed to be strongly downregulated in all ALS patients. These findings offer a potential marker for the stratification of FTLD patients and ALS patients with FTLD comorbidity.

| | Cohort Demographics | | |
|---|---|---|---|
| A-L: Axial and Limb Onset<br>B-L: Bulbar and Limb Onset<br>A-B: Axial and Bulbar Onset | **ALS Spectrum** | **FTLD** | **Healthy Control Donors** |
| | (n = 208) | (n = 42) | (n = 58) |
| **Sex** | | | |
| Female | 95 (45.7%) | 18 (42.9%) | 28 (48.3%) |
| Male | 113 (54.3%) | 24 (57.1%) | 30 (51.7%) |
| **Tissue Site** | n = 451 | n = 42 | n = 93 |
| Frontal Cortex | 193 (42.8%) | 42 (100%) | 56 (60.2%) |
| Lateral Motor Cortex | 104 (23.1%) | 0 | 18 (19.4%) |
| Medial Motor Cortex | 102 (22.6%) | 0 | 19 (20.4%) |
| Motor Cortex Unspecified | 52 (11.5%) | 0 | 0 |
| **ALS Subtype** | | NA | NA |
| ALS-Glia | 33 (15.9%) | – | – |
| ALS-TD | 56 (26.9%) | – | – |
| ALS-Ox | 89 (42.8%) | – | – |
| ALS-Discordant | 30 (14.4%) | – | – |
| **Disease Duration (months)** | | Not Available | NA |
| ALS-Glia | 29.1 ± 3.81 | – | – |
| ALS-TD | 38.1 ± 3.40 | – | – |
| ALS-Ox | 41.8 ± 3.18 | – | – |
| ALS-Discordant | 42.4 ± 6.35 | – | – |
| **Age of Onset (years)** | | Not Available | NA |
| ALS-Glia | 63.2 ± 1.83 | – | – |
| ALS-TD | 62.7 ± 1.68 | – | – |
| ALS-Ox | 60.4 ± 1.16 | – | – |
| ALS-Discordant | 60.9 ± 1.87 | – | – |
| **Site of Onset** | | NA | NA |
| ALS-Glia | Bulbar: 11; Limb: 20; Unknown: 2 | – | – |
| ALS-TD | Bulbar: 17; Limb: 35; Axial: 2; A-L: 1; Unknown: 1 | – | – |
| ALS-Ox | Bulbar: 23; Limb: 51; Axial: 2; A-B: 1; A-L: 1; B-L: 4; Generalized: 1; Unknown: 6 | – | – |
| ALS-Discordant | Bulbar: 8; Limb: 19; Unknown: 2; A-B: 1 | – | – |
| **Age of Death (years)** | | 66.5 ± 9.5 | 64.8 ± 15.7 * |
| ALS-Glia | 66.1 ±1.60 | – | – |
| ALS-TD | 66.7 ± 1.33 | – | – |
| ALS-Ox | 64.0 ± 1.05 | – | – |
| ALS-Discordant | 64.0 ± 1.65 | – | – |
| **FTLD Comorbidity** | 27/208 (13.0%) | 42/42 (100%) | NA |
| ALS-Glia | 6/33 (18.2%) | – | – |
| ALS-TD | 8/56 (14.3%) | – | – |
| ALS-Ox | 10/89 (11.2%) | – | – |
| ALS-Discordant | 4/30 (13.3%) | – | – |

* Three healthy control samples had an age of death listed as "90 or Older". A conservative estimate of 90 years was used for all samples listed as such.

**Table S1. Cohort demographics (also provided as separate file)**
Cohort demographics for ALS patients, neurological controls, and healthy controls. Disease Duration, Age of Onset, and Age of Death metrics presented as mean ± standard error.

**Table S2. Sample IDs (separate file)**
GEO IDs and metadata for all postmortem cortex transcriptomes considered in this analysis.

**Table S3. Transposable Element Quantification (separate file)**
Transposable element raw counts for all samples considered in this analysis. TE counts reflect the application of the expectation maximization algorithm, to aid in the allocation of multi-mapping reads.

**Table S4. Resource, software, and data sources (separate file)**
Resource, software, and data sources for the ALS patient stratification analysis performed in this study.

**Table S5. Enrichment feature set (separate file)**
Normalized gene and TE counts for the 1681 features considered during enrichment, network development, and univariate analysis. Feature counts are provided for both the ALS cohort and controls.

**Table S6. TE names corresponding to Fig. 2D (separate file)**
Row names for the 426 unique transposable elements presented in Fig. 2D.

**Table S7. WGCNA analysis of TEs (separate file)**
Application of WGCNA to a feature set containing transposable elements exclusively. TE eigengenes do not show correlated expression at the subfamily, family or superfamily level – supporting the consideration of locus-specific TEs as unique molecular features.

**Table S8. Eigengene membership (separate file)**
Eigengene memberships and gene significances are provided in the context of three clinical parameters: disease duration, age of symptom onset, and age at death.

**Table S9. Eigengene enrichment for gene ontology (separate file)**
Enrichment of eigengenes for biological process, molecular function, and cellular component gene ontologies. Bonferroni-adjusted *p*-values are provided and used to assess significant associations between eigengenes and gene ontologies.

**Table S10. ALS patient subtype assignment and clinical data (separate file)**

Assignment of ALS patient subtype labels, using the majority agreement approach outlined in Tam et al.[7]. Clinical parameters, such as site of onset, age of onset, age at death, disease duration, fALS genetic characterization, and disease group, are provided for each ALS patient.

| Concordance Matrix | | Eshima et al. | | |
|---|---|---|---|---|
| | | ALS-TD | ALS-Ox | ALS-Glia |
| Tam et al.[7] | ALS-TE | **21** | 6 | 0 |
| | ALS-Ox | 9 | **79** | 1 |
| | ALS-Glia | 1 | 4 | **19** |

**Table S11. Subtype concordance matrix (also provided as separate file)**
Subtype concordance matrix highlights the strong agreement of subtype labels (85%) between this analysis and the foundational work from Tam et al.[7] for the 140 samples in common.

**Table S12. Differential expression (separate file)**
Pairwise differential expression analysis for ALS subtypes and controls. A multi-factor design equation was utilized for this analysis, accounting for sequencing platform and disease subgroup. A full list of subtype-associated features is also provided and provides the ALS subtype assigned to each feature during clustering with the NovaSeq and HiSeq cohorts.

**Table S13. Sample subtype assignment (separate file)**
Robustly assigned subtype labels are provided for all 451 ALS patient samples considered in this analysis.

**Table S14. Network edge weights for VisANT (separate file)**
WGCNA derived edge weights for eigengene network visualization in VisANT.